Molten polystyrene structures above the glass transition, T > Tg
Utracki, L. A.; Sammut, P.

National Research Council Canada   Conseil national de recherches Canada

Canada

Molten Polystyrene Structures Above the Glass Transition, $T > T_g$

L. A. Utracki, P. Sammut

National Research Council Canada, Industrial Materials Institute, 75 de Mortagne, Boucherville, Quebec, Canada J4B 6Y4

Correspondence to: L. A. Utracki (E-mail: leszek.utracki@cnrc-nrc.gc.ca)

ABSTRACT: The old controversial idea of structures in molten amorphous polymers is being accepted with theoretical and experimental evidence. Wool's twinkling fractal theory of the glass transition and recent atomic force micrographs are convincing proof of the dynamic, solid aggregate presence below and above T_g. This article offers detailed analysis of the experimental data from high-pressure dilatometry, as well as from the oscillatory shear tests in the glassy and the molten state of polystyrenes. The results indicate the presence of a transient structure at $T > T_g$; transient as it depends on the structure of the vitreous polymer and the rate of heating it across T_g. Thus, molten polymer is not always at the thermodynamic equilibrium. © 2011 National Research Council Canada.[†] J Polym Sci Part B: Polym Phys 49: 1369–1380, 2011

KEYWORDS: compressibility; dynamic moduli; equation-of-state; polystyrene; rheology; thermal expansion

INTRODUCTION The glass transition temperature (T_g) is considered a boundary between the vitreous and molten phase. It is recognized that glass is a supercooled liquid, not at thermodynamic equilibrium, and as the temperature decreases from T_g there are several glass/glass transitions all the way to the reduced quantum temperature, $\tilde{T} \cong 0.004$, or $T \approx 50–80$ K.[1] Similarly, in the molten phase above T_g there are liquid/liquid transitions, kinetic or thermodynamic in nature (e.g., melting of syndiotactic dyads in polyvinyl chloride), which depend on temperature T, pressure P, time t, and so forth.[2] Boyer has been a persistent proponent of the liquid–liquid transition temperature (T_{LL}) above which "entire polymer chain is free to move as a unit."[3–5] Transitions usually indicate some change of the molecular mobility and/or structures. The kinetic nature of T_g is reflected not only in the well-recognized diversity of glass behaviors but also in properties of molten polymer within the temperature span: $T_g < T < T_c$, where $T_c \approx T_{LL}$ is the crossover temperature; $T_c/T_g \approx 1.25 \pm 0.10$.[6–9]

According to Götze and Sjogren, T_c is readily observed by neutron scattering and other vibrational spectra, and it appears in molecular modeling. Furthermore, T_c, "seems to be an equilibrium parameter of the system, which separates the supercooled liquid state in two regions."[10] The molecular modeling and dynamic measurements established several relaxation modes at $1 < T/T_g < 1.6$, which affect the T and P dependencies of liquid viscosity or relaxation time.[11–14] At $T < T_c$, the mode-coupling theory (MCT) considers liquid as an assembly of particles enclosed in cages formed by their neighbors with vitreous-type α-relaxation controlling the behavior, whereas at $T > T_c$, the molecular vibrations dominate.[15,16] In other words, cooling the liquid involves two relaxation mechanisms—segmental (at $T > T_c$) and structural (dominant at $T < T_c$). Their crossover at T_c depends on the fragility index of the glass-forming liquid, m:

$$m = \left(\frac{1}{T_g}\right)\left(\frac{\mathrm{d}\log\eta}{\mathrm{d}(1/T)}\right)_{T=T_g} \quad (1)$$

The T_c/T_g ratio ranges approximately from 1.6 (for B_2O_3 where $m = 32$) to 1.35 (for polyisobutylene, PIB where $m = 49$) and 1.15 [for polystyrenes (PS) where $m = 139$].[8,9,17–19] It is noteworthy that m also increases with the number average molecular weight, M_n (e.g., for PS from $m \approx 70$ to 145 for $M_n = 0.5$ to 3000 kDa) and so does the T_c/T_g ratio.

The polymer dynamics at $T < T_c$ is complicated by other relaxation processes such as the fast and the elementary. The former, which originates in backbone chain vibrations or side group's motion, starts in the vitreous state near the Vogel-Fulcher-Tammann-Hesse (VFTH) temperature T_0 and ends above T_c. The elementary relaxations (only in molten polymers) are related to conformational transitions, which extend to temperatures well above T_c.[13,20,21]

In 2008, Wool proposed the twinkling fractal theory (TFT), which postulates that solid-percolating fractal structures form in liquids cooled from $T > T_c$.[22] The theory was derived from the Boltzmann population of excited states in the anharmonic intermolecular potential between atoms, coupled with percolating solid fractal structures near T_g. Noteworthy, a similar model of a dual nature for molten amorphous polymers was discussed by Robertson already in his 1975 review.[23] At that time, the evidence was based on X-ray or neutron scattering (X-ray diffraction (XRD), small angle X-ray scattering (SAXS), and small angle

neutron scattering (SANS)) and on a variety of electron micrographs. The reported grain sizes ranged from about 3 to 200 nm; after quenching the initially small grains grew during annealing by a factor of about five.

TFT predicts that the temperature-dependent volume fraction of solid and liquid (ϕ_s and ϕ_L, respectively) follows the relations:

$$\left.\begin{array}{c} \phi_L = (1 - p_c)(T/T_g) \\ \phi_L + \phi_S \equiv 1 \end{array}\right\rangle \Rightarrow \left\langle\begin{array}{l} T = 0(K)_c \Rightarrow \phi_{L,0} = 0 \\ T = T_g \Rightarrow \phi_{L,g} = 1 - p_c \\ T \rightarrow T_c \Rightarrow \phi_{L,c} = (1 - p_c)T_c/T_g \rightarrow 1 \end{array}\right.$$

(2)

where p_c is the rigidity percolation threshold. Accordingly, the solid-like aggregates first appear near T_c. The glass transition (T_g) occurs when the solid fraction of aggregates reach the rigidity percolation threshold, $\phi_{S,g} \equiv 1 - \phi_{L,g} = p_c$, while complete solidification is expected only at absolute zero, $T \rightarrow 0$ K. Physics recognize several values of the percolation threshold, for example, for perfect crystalline packing, for random packing of uniform spheres, for anisometric particles with variable aspect ratio, and so forth. Consequently, like p_c, T_g is also controlled by such quantities as geometry (e.g., dimensionality, packing arrangement, and segmental aspect ratio), as well as on the thermodynamic interactions, on three-dimensional flow stresses and strains, rate of temperature changes, pressure effects, and so forth. For example:

- Face-centered cubic and hexagonal close-packed, $z = 12$:[24] $p_c^{fcc} = 0.120164 \pm 0.000001$
- Body-centered cubic, $z = 8$: $p_c^{bcc} = 0.2459615 \pm 0.0000010$
- Experimental data for polydispersed spherical drops: [25] $p_c^{spheres} = 0.18 \pm 0.03$

Assuming that, on cooling, the solid aggregates start forming at T_c, then from the experimental values of $T_c/T_g = 1.15$ and 1.35 (for PS and PIB, respectively) one calculates $p_c^{spheres} = 0.13$ and 0.26, bracketing the values observed in immiscible polymer blends.[25] Accordingly, while T_c is MCT-derived equilibrium parameter, T_g is a dynamic macrotransition controlled by critical percolation of segmental or molecular aggregates. T_g is considered isoviscous, but it is not iso-free volume state, and volume changes at T_g have been reported early.[26] Furthermore, T_g in reduced variables: $\tilde{T}_g \equiv T_g/T^* \neq$ const. (T^* is the equation of state scaling temperature, characteristic for the given polymer); thus, the transition is not the corresponding state variable, as, for example, is the critical point.[27–30]

Recently, Wool and his coworkers used the atomic force microscopy (AFM) in the tapping mode for detecting the percolating twinkling fractal solid aggregates in PS below and above T_g.[31,32] As tapping-mode AFM detects local variation of substrate rigidity, it indeed provides a direct evidence for the presence of twinkling rigid clusters in liquid matrix. The twinkling frequency:

$$\omega(T) = \omega_o \exp\left\{-\frac{\beta(T^{*2} - T^2)}{kT}\right\}$$

(3)

($\omega_o \simeq 1$ THz is the lowest fundamental frequency of the solid cluster) depends on T, which through the population of intermolecular oscillators controls the cluster size, observed by AFM as ranging from 4 to 40 nm (note the relative agreement with about 40-year-old data[23]). The two-dimensional correlation coefficient decreases with time and temperature indicating increasing randomness of the aggregate formation, as evident already at $T_g + 10$ K. The fractal dimension of about 1.88 well agrees with the theory.

TFT is an intriguing concept, which may clarify many conflicts surrounding the glass transition in amorphous polymers. At the same time, its implications are serious and disturbing. The fundamental postulate is the progressive increase of solid cluster population from zero near T_c to totality at absolute $T = 0$ (K). Accordingly, T_g seems almost an accidental transition, subjected to all the variables that affect percolation threshold, that is, formation of an infinite cluster. The cooling takes the equilibrium liquid at $T > T_c$ to nonequilibrium glass at $T < T_g$. However, where during the cooling the nonequilibrium structure first appears? Up to the present time, the melts above T_g have been treated as equilibrium liquids with the experimental data interpreted by equilibrium theories—Is this treatment valid? Furthermore, if the melt structure is not at equilibrium, how much the performance of the processed article depends on the structure of vitreous pellets and processing parameters? Consequently, this article focuses on the molten PS just above T_g. The aim is to examine if different liquid cooling or heating kinetics affect the physical properties of the polymer at $T_g < T < T_c$. This can be done by observing the effects of temperature changes in thermodynamic or rheological tests, such as pressure–volume–temperature (PVT) measurements, or oscillatory shearing versus T of the solid and molten polymer near T_g.

Zoller and Walsh in their book described four PVT test procedures that under condition of the thermodynamic equilibrium should yield the same dependence. Thus, one may carry the PVT measurements isobarically or isothermally, either increasing or decreasing T and/or P.[33] However, the presence of dynamic clusters at $T_g < T < T_c$ suggests a possibility of progressively changing behavior with the distance from the critical percolation volume fraction. As derivatives are more sensitive than the functions, in addition to $V = V(P, T)$ the thermal expansion and compressibility coefficients, (α and κ, respectively) should be analyzed:

$$\alpha \equiv \left(\frac{\partial \ln V}{\partial T}\right)_{T^0,P,q}; \kappa \equiv -\left(\frac{\partial \ln V}{\partial P}\right)_{P^0,T,q}$$

(4)

In this general relation for vitreous state, P^o and T^o are the glass formation pressure and temperature, respectively with q being the rate of heating or compressing; evidently, for equilibrium liquids only P and T, respectively, is important.[34]

Although the PVT measurements explore the influence of T and P on V and its derivatives, the dynamic rheological tests are done only at ambient pressure, scanning PS response while varying the temperature across T_g, from the vitreous to liquid phase or vice versa. The dynamic temperature

TABLE 1 Polymers Studied in this Work

No.	Polymers	Manufacturers	M_w (kDa)	M_n (kDa)	T_g (K) $\pm$ 0.1	Refs.
1	PS-686	Dow Chem	279	90.7	368.4	35
2	PS-667	Dow Chem	352	215	361.0	34, 36, 37
3	PS-1301	Nova Chemicals	270	–	378 $\pm$ 0.2	38, 39
4	PS-220	Nova Chemicals	216	56	360.8	40

Note: PS-667 contains 700 ppm Zn-stearate and 2.5% of mineral oil; PS-686 and PS-1301 are lubed grades.

sweep of molten polymer can be carried out by heating and then cooling. Unfortunately, because of the exponential viscosity increase on cooling toward T_g, these tests cannot extend closer than about $T_g + 20$ °C.

EXPERIMENTAL

Polystyrene

PVT behavior of PS has been studied following different test procedures. The data covering a wide range of T and P will be analyzed directly, without recourse to theory. The PS grades used in this study are listed in Table 1. The weight and number average molecular weights, M_w and M_n, respectively, were determined by size exclusion chromatography (SEC), calibrated using toluene solutions of narrow molecular weight, anionic PS. In commercial PS the polydispersity index ranged broadly, viz., $M_w/M_n = 1.63$–3.85. Furthermore, they do contain different type and amount of lubricants. The materials have been tested "as received," without purification.

PVT Tests

Excepting PS-686 (Styron®-686, studied in a specially constructed bellows dilatometer) other *PVT* data were obtained using Gnomix™ — a commercial, high-pressure dilatometer from Gnomix, Boulder, CO. PS-686 was measured isobarically by cooling from about 200 to 8 °C, remelting to 200 °C, annealing there for about 2 h, increasing P, and stepwise cooling at 10 °C/min to the lowest T.[35] Also, PS-677 was measured isobarically but by slow heating from about 30 to 250 °C in 170 T-steps, each lasting about 25 min. After the maximum temperature was reached, the sample was cooled, the pressure was increased by 30 MPa, and then the next isobaric heating step commenced for the total of 71 h automatic test run. PS-677 and PS-1301 were tested isothermally, starting at the lowest T and P. At each T-level, the pressure was increased from about 10 to 190 MPa in steps of 30 MPa, then temperature increased by about 10 °C, and so forth. This procedure is considered "standard."[33]

Thus, during the isobaric run at each selected P, the volume gradient, ΔV, is measured from the highest to the lowest T (or vice versa), then the material is cooled down to the lowest T, another pressure is set in, and ΔV is measured up to the highest T, and so forth. By contrast, during the isothermal measurements at each selected temperature, P is stepwise increased from the lowest to the highest value; thus, the sample sees the top T and P only at the end of the test. These different methods of measurements affect volume changes of the vitreous phase but not that of equilibrium liquid. However, one may pose a question: under which conditions (time, t, T and P) the molten polymer on cooling or pressurizing departs from the thermodynamic equilibrium?

Rheological Tests

The viscoelastic properties across the glass transition region were measured in a dynamic–mechanical thermal analyzer (DMTA V, Rheometric Scientific) in a single cantilever bending mode. For these tests, the dried (under dynamic vacuum at 55 °C for $\geq$ 72 h) PS-1301 pellets were molded at 200 °C into rectangular specimens: for 8 min without pressure, compressing for 1 min at $P = 3.2$ MPa, and then cooling in one of these sequences:

1. The quenched specimens (qu) were prepared by heating the polymer in steel tooling for 9 min at 200 °C in a molding press and then removing the steel tooling from the mold and immersing it in cold water (ca. 15 °C).
2. The slow-cooled specimen (sl) remained in the press at $P = 3.2$ MPa during cooling to room temperature (RT) in about 10 min, while the free cooling rate decreased from the initial 35 to 5 °C/min.
3. The annealed specimen (an) were prepared following the same procedure as that for sl, but in addition, they were placed in a vacuum oven at 90 °C for 3 h, and then with power cutoff slowly cooled to RT in about 1.5 h.
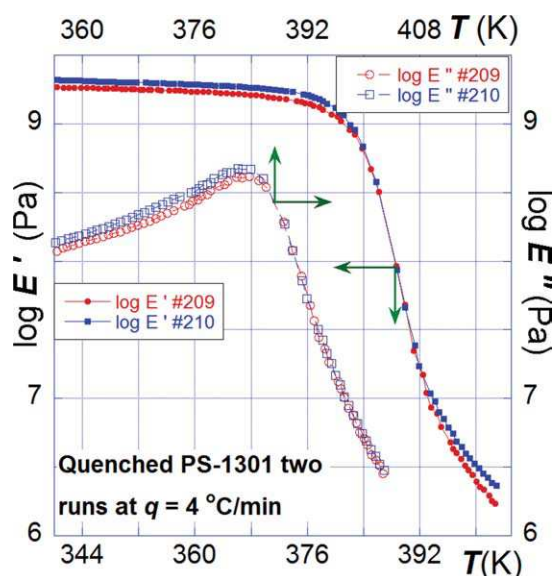

FIGURE 1 Storage and loss tensile moduli of quenched PS-1301 at the heating rate, q = 4 °C/min and frequency $\omega = 1$ rad/s.
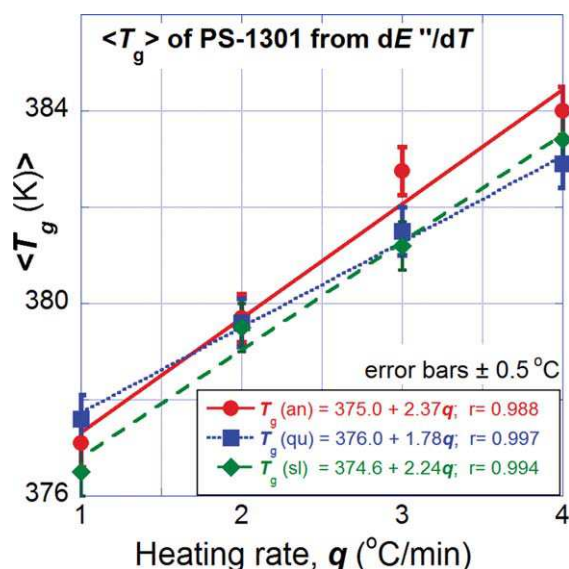
FIGURE 2 Average T_g of the annealed (an), quenched (qu) and slow-cooled (sl) of PS-1301 versus q at frequency $\omega = 1$ rad/s.

The specimens were stored at RT $\approx 22\ °C$, that is, below the beta-transition temperature, $T_\beta \approx 51\ °C$, thus avoiding the danger of structural changes by physical aging at $T_\beta < T < T_g$.

The DMTA temperature scans were carried out at frequency $\omega = 1$ rad/s, at constant heating rates: $q = 1, 2, 3,$ or 4 $°C/$min and at T ranging from about 30 to 130 $°C$. The run-time ranged from 100 to 25 min with the corresponding reduction of the number of data points from 600 to 150. Reproducibility is illustrated in Figure 1. T_g was determined by numerical differentiation of the dynamic loss (E'') modulus (see Fig. 2), plotting the derivative versus T and then finding the temperature, $T = T_g$, at which: $\left[\mathrm{d} \ln E''/\mathrm{d}T|_{T-T_g} \right] = 0$. Evidently, T_g depends on ω, the specimen preparation and q, but as the experiments were performed at $\omega = $ const., the transition depended only on the preparation method and q (see Fig. 2) with an error of $\Delta T_g \approx \pm 0.5\ °C$, decreasing with increasing q to about $\pm 0.2\ °C$.

The oscillatory shearing of molten PS was carried out in an advanced rheometric expansion system (ARES-LS with 25-mm parallel plates) at $\omega = 0.1$ or 1.0 rad/s (0.0159 or 0.1592 Hz) and strain $\gamma = 5\%$. The test specimens were compression molded and slow cooled into circular discs, 25 mm in diameter and 0.7–2.0 mm thick. The specimen thickness was not affected the results. The PS pellets were dried under dynamic vacuum for 72 h at 60 $°C$. The specimens were subjected to a four-step programmed temperature ramping:

1. Applying the initial compressive force of 10 or 100 g for 120 s;
2. Increasing T from 110 to 200 $°C$ at 1 or 2 $°C/$min;
3. Annealing for 10 min at 200 $°C$;
4. Decreasing T from 200 to 116–118 $°C$ at the rate of 1 or 2 $°C/$min.

For compensating the effects of tooling thermal expansion, the instrument was programmed for correcting it at $T >$ 90 $°C$ at a rate 2.6778 μm/$°C$. The recovered samples were smooth, slightly deformed and without discoloration, cracks or gas bubbles.

RESULTS

PVT Data
Figure 3 displays ln$V$, α and κ for PS-686, PS-667 and PS-1301 at low ($P = 0.1$ or 10 MPa) and high ($P = 160$ or 190 MPa) pressures. For the ease of comparison, Figures 3(A)–3(D) is drawn on the same scale. The T_g's reported in the original publications (refs. 35–39) are also marked. The data points for ln$V$ are experimental; those for α and κ were numerically computed using the nine-point moving-arch procedure.

The three polymers were tested following different procedure:

- PS-686 was tested isobarically, decreasing T (rapid cooling),
- PS-667 was tested isobarically, increasing T (slow heating),
- PS-1301 was tested isothermally, increasing T (slow heating).

These three sets of *PVT* data were selected from between nearly 100, measured on the same instrument by the same technical officer more than 20 years or so. These data are presented for demonstrating the typical differences caused by different test procedures, especially within the transition region, **T**. In addition to the procedure, the rate of heating or cooling may also influence the results (see Experimental section).

The ambient pressure glass transition is insensitive to the test methods, but the derivatives, α and κ, show significant differences, especially within the transition zone **T** at $T \leq T_g$. The transition region is the largest for isobaric cooling [Fig. 3(A)] and the smallest for the isobaric heating [Fig. 3(B)]. The standard test procedure, illustrated in Figure 3(C), leads to an intermediate distortion. The compressibility coefficients, κ [Fig. 3(D)] show a similar behavior as α. However, it is noteworthy that within the vitreous and molten regions α is nearly independent of T, while κ increases with it; both coefficients decrease with P.

Oscillatory Shearing across T_g
For the viscoelastic testing in DMTA, the molded PS-1301 specimens were annealed (an), quenched (qu), or slow cooled (sl). As T_g vary slightly with the specimen preparation method, the abscissa was expressed in relative terms as $T_r = T/T_g$. Example of the results is displayed in Figures 4(A)–4(D) for $q = 1$ and 3 $°C/$min, respectively.

Figure 5 shows the difference between the quenched and annealed moduli for the three heating rates, $q = 1, 3,$ and 4 $°C/$min. The relative storage modulus, G', is about 50% larger than that of loss, G'', but they both show a similar tendency: the largest ratio is observed for the fastest heating
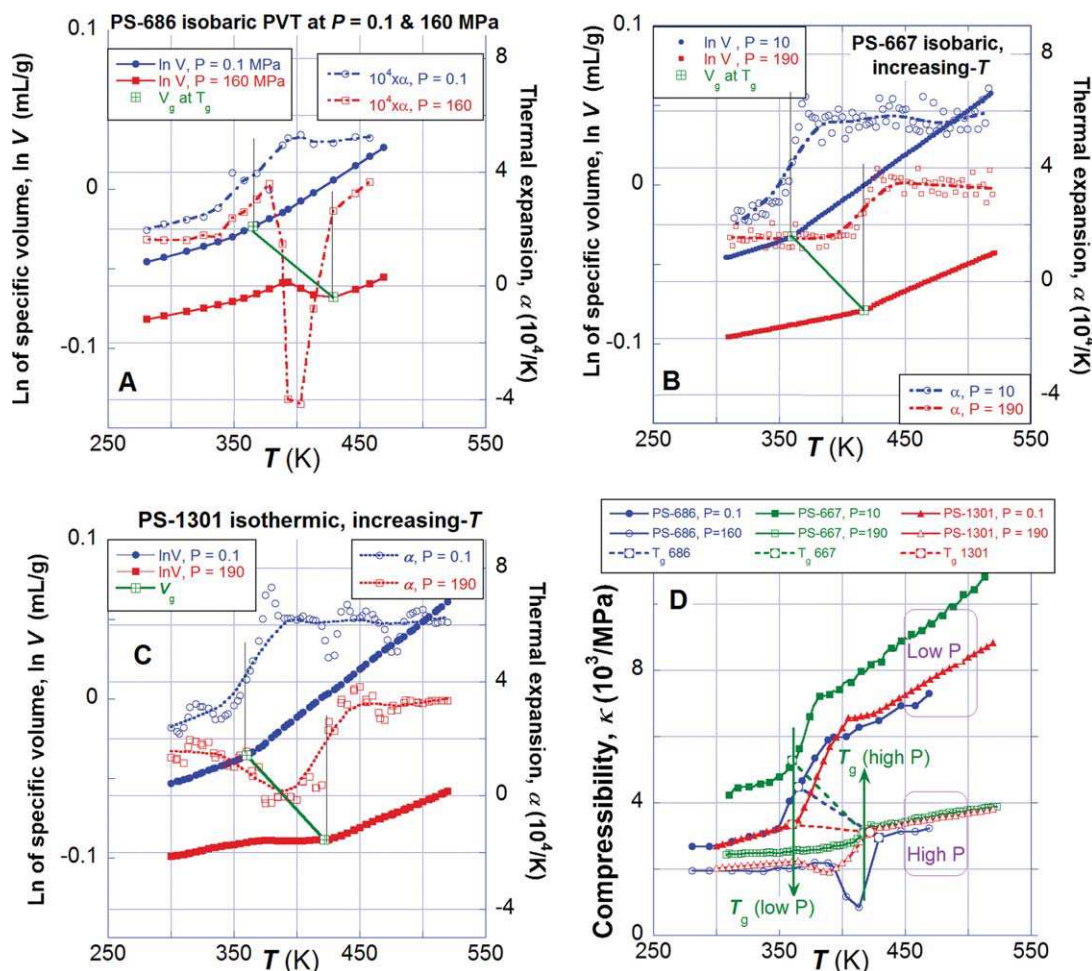
FIGURE 3 (A–C) Temperature dependence of specific volume, V, and the thermal expansion coefficient, α, at nearly ambient and high pressures for PS-686, PS-667 and PS-1301, respectively, each tested following different *PVT* test procedure. (D) displays the compressibility coefficient, κ, for the three polymers. The lines represent smoothed α and κ, data. The vertical T_g lines are from the original publications.

and the shortest annealing time during the *T*-sweep. At the lowest temperatures, $T \leq T_g - 75(K)$ (i.e., below the beta transition, T_β) the glass moduli are independent of the specimen preparation method—an, qu, or sl; the differences displayed in Figure 5 only appear at $T > T_\beta$, especially in vicinity of the glass transition.

Melt Rheology

For the tests at close proximity of T_g, the low molecular weight PS-220 was selected. The DMTA data at $\omega = 1$ rad/s indicated that T_g(PS-220) = 360.8 ± 0.1 K. Before the temperature sweeps, the thermal stability was examined at frequency $\omega = 6.28$ rad/s and $T = 473$ K — the 2-h testing proved that the polymer was thermally stable.

The dynamic temperature sweeps of molten PS-220 were carried out in ARES at the conditions listed in Table 2. The measurements may be grouped into three series: (I) tests at frequency $\omega = 1$ rad/s; (II) tests at $\omega = 0.1$ rad/s using variable gap height; (III) tests at $\omega = 0.1$ rad/s and about constant sample thickness. Considering large *T*-span, the

starting temperature was 110 °C, that is, about 22 °C above T_g. Loading the specimens at this temperature required application of vertical (normal) force. Unfortunately, ARES does not have settings for, or readings of, the normal force during specimen loading; thus. its magnitude could not be precisely measured and reproduced. The three temperature ramping rates (1, 2, or 3 °C/min) had a negligible effect on the results. The examples of data are displayed in Figures 6(A)–6(D).

DISCUSSION

For decades, the glass transition was considered a boundary between the physically different states of matter; a liquid at thermodynamic equilibrium above T_g and a nonequilibrium glass below T_g, the latter characterized by a spectrum of physical properties dependent on the preparation method. [35,41] The recent studies raise an impertinent question if indeed the liquids above T_g are at equilibrium. In particular, the TFT and the reported AFM images of predicted solid clusters, force such a question. [22,31] The theory
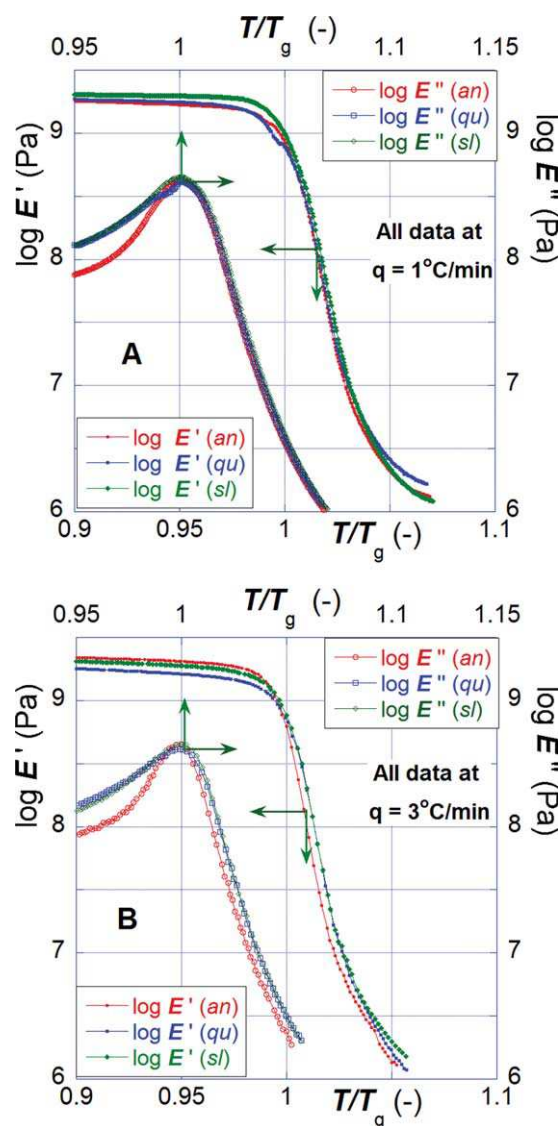
FIGURE 4 Storage and loss tensile moduli versus reduced temperature for the scan rate 1 and 3 °C/min in plot (A) and (B), respectively. Behavior of specimens prepared by annealing (an), quenching (qu) or slow cooled (sl) are shown.

variables (e.g., pseudocrystalline structure of the aggregate, aspect ratio of the aggregating elements, binary interactions, cooling kinetics, pressure, etc.), *per se*, the TFT model implies multiplicity of structures and performances not only below but also above T_g. One must consider the possibility that the nonequilibrium state is not limited to glass at $T < T_g$, but it extents some distance into the liquid region at $T > T_g$. It is noteworthy that the TFT autocorrelation function depends on time and temperature, thus the nonequilibrium state of melt at $T_g < T < T_c$ is an inherent part of the theory.[32] In other words, at $T < T_c$, the melt structure depends on thermodynamics and kinetics, the rate of changes slowing down as the temperature decreases. One may expect that these changes may stop at $T < T_{\beta}$.[42]

This article analyzes the material behavior in the vicinity of T_g using three types of macroscale measurements: (1) *PVT* on both sides of T_g; (2) The viscoelastic *T*-scan starting
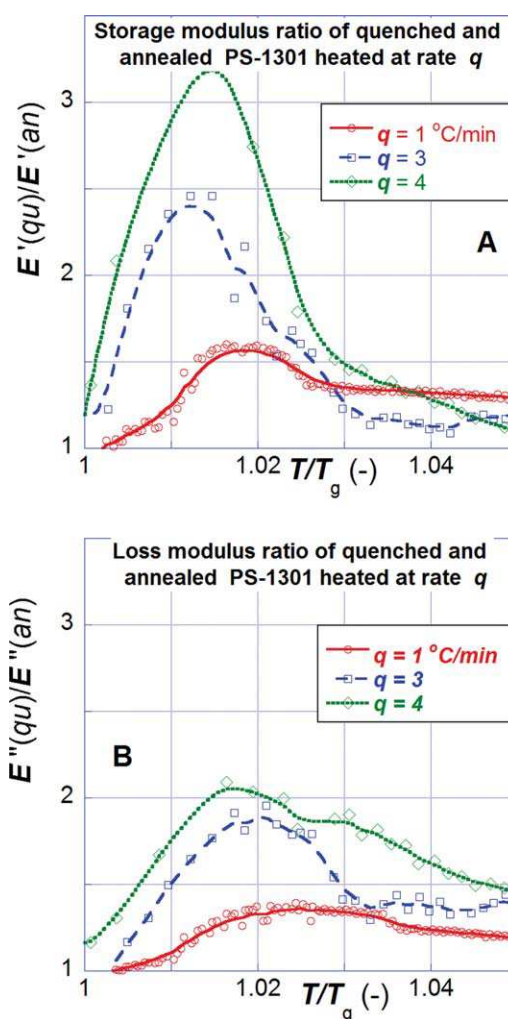
FIGURE 5 Relative dynamic moduli versus relative temperature for quenched (qu) and annealed (an) PS-1301 specimens. (A) and (B) show the relative storage and loss tensile moduli, $E'(\text{qu})/E'(\text{an})$ and $E''(\text{qu})/E''(\text{an})$, respectively.

diminishes the importance of T_g—it is no longer a boundary between two thermodynamically different states, but a percolation phenomenon, an outcome of progressive crowding of solid aggregates on the way from the melt at $T \approx T_c$ (where $\phi_s = 0$) to total solidification ($\phi_s = 1$) at absolute zero. Qualitatively, the material state is the same above and below T_g, but the only difference being the size of twinkling clusters. In other words, TFT considers that on cooling from above T_c, melts transform into suspensions of twinkling solid aggregates with concentration at T_g reaching the percolation threshold, p_c. In consequence, the vitrification process resembles a formation of infinite clusters in suspensions that leads to solidification at the maximum packing volume fraction: $\lim_{\phi \to \phi_m} \eta_o = \infty$. Thus, since like ϕ_m, p_c also depends on several

TABLE 2 Summary of Conditions for the Dynamic Shear Tests of PS-220

#	Run #	h	ω	q	F_c	T (°C)	T_c (°C)	T_{peak} (°C)	Shapes
1	231	1.717	**1**	2	≤10	110-200-110	136/138	136.5	Peak
2	232	1.796	**1**	2	≤100	110-200-110	131/136	136.5	Shoulder
3	237	1.698	**1**	3	≤10	110-200-110	145/140	–	Peak
4	240	1.717	0.1	2	–	110-200-110	136/140	–	Shoulder
5	240-2	1.811	0.1	**1**	≤100	110-150-110	127/135	135	Peak
6	241	0.744	0.1	**1**	≤10	110-150-110	138/142	–	Peak
7	242	0.930	0.1	**1**	≤10	110-200	146/–	145	Peak
8	243	0.970	0.1	2	≤10	110-200-110	145/146	–	Peak
9	258	0.884	0.1	2	≤10	110-200-110	144/146	143	Peak
10	259	0.844	0.1	2	≤10	110-200-110	146/146	141	Peak
11	260	0.909	0.1	2	≤100	110-200-110	146/146	146	Peak

Differentiation of the dynamic moduli ($\omega = 1$ rad/s) from runs #231–237 (shown in bold) show slope change at $T_c = 140 \pm 2$ °C $= 413 \pm 2$ K, that is, $T_c/T_g = 1.145 \pm 0.005$.

Notes: h = gap between parallel plates; ω = frequency (rad/s); q = heating rate (°C/min); F_c = initial compressive force (g); T_c = crossover temperature for heating and cooling (°C); T_{peak} = derivative peak position (°C); shape of the rheological function (e.g., G' or η^*) versus T.

below T_β and stretching to $T \approx 1.07T_g$; and (3) Oscillatory shear flow of molten PS at $T > T_g + 22$. To avoid prejudicing the interpretation, the experimental data were analyzed directly and their derivatives computed numerically. In the following section, the behavior of amorphous PS will be discussed progressing from the lowest to the highest temperature.

The Vitreous Phase

The initial viscoelastic tests were carried out as the T-sweep from −40 °C to $T > T_g$, thus from well below T_β to above T_g. Within the range of temperatures: $0.72 \leq T/T_g \leq 0.87$, the dynamic moduli were found to be independent of the specimen preparation method: an, qu, or sl. Only above the upper limit, being just above $T_\beta = 0.86T_g$, the differences in molecular mobility between the three types of specimens begun. Consequently, the following viscoelastic scans were conducted starting at +30 °C, that is, the same as that for *PVT* tests. Thus, for both type of measurements, the beta transition, $T_\beta \approx 51$ °C, was very near the initial temperature for allowing its precise determination. The work, as planned, focused on the glass transition region.

The Glass Transition Region

This region was probed by the *PVT* and viscoelasticity measurements conducted, respectively, in a range of $0 \leq P$ (MPa) ≤ 190 and at ambient P. The *PVT* data illustrate importance of the rate, and the temperature change during scanning across the T_g region. Because of the time scale, the viscoelastic measurements more directly revealed the presence of liquid structures above T_g.

The *PVT* data provide unique information on the P-effects on the melt structure. Figure 3 displays the T-dependence of specific volume, $V = V(P, T)$, the thermal expansion coefficient, α, and the compressibility coefficient, κ, for the three PS resins:

1. PS-686 was measured isobarically, starting at $T_g + 30$ °C, annealing there for 2 h, then cooling at 10 °C/min down to 7.7 °C; see Figure 3(A).[35,43]

2. PS-667 was measured isobarically (as well as isothermally—not shown), by heating from 30 to 250 °C at a rate of about 0.05 °C/min; see Figure 3(B).[34,36,38]

3. PS-1301 was measured isothermally following the standard procedure, that is, by heating from 30 to 250 °C at a rate of 0.05 °C/min; see Figure 3(C).[38,39]

For clarity, only two isobaric curves are displayed in Figures 3(A)–3(C). First, let us focus on the low pressure ($P \leq 10$ MPa) results. The rapid cooling of PS-686 in Figure 3(A) makes T_g indistinguishable on $\ln V$ curves. The thermal expansion coefficient α is constant in the melt but then continuously decreases on cooling below T_g. The compressibility coefficients κ [Fig. 3(D)] indicate that T_g is shifted to slightly higher T than these determined for other polymers. The $\ln V$ and α-coefficients of PS-667 and PS-1301, measured isobarically or isothermally, follow nearly identical T-dependencies, that is, the isothermal or isobaric slow heating at low pressures generates similar $\ln V$ and α dependencies. The latter coefficient increases with T across the glass transition region up to $T_c \approx 1.14T_g$, where it becomes nearly constant, marking the beginning of the equilibrium liquid. By contrast, κ of PS-667 and PS-1301 are apart, the former polymer having significantly larger compressibility than the latter. As the isothermal data confirm the discrepancy, the reason for the lack of superposition may be the large quantity of two lubricants (see Table 1).

The differences between the three sets of data are more significant at higher pressures. Rapid isobaric cooling of PS-686 [Fig. 3(A)] results in abnormal volume increase near T_g, evident in $\ln V$, α and κ [Fig. 3(D)] plots. Hellwege et al.[44] and later Breuer in his unpublished dissertation (summarized in ref. 45) also used isobaric cooling, obtaining similar results to these shown in Figures 3(A) and 3(D). The abnormal volume expansion was explained by the high rate of cooling, that is, caused by a thermodynamic nonequilibrium of the melt that overshoot the equilibrium volume change with temperature (an entropic effect).[35] If so, the end point of the straight line of
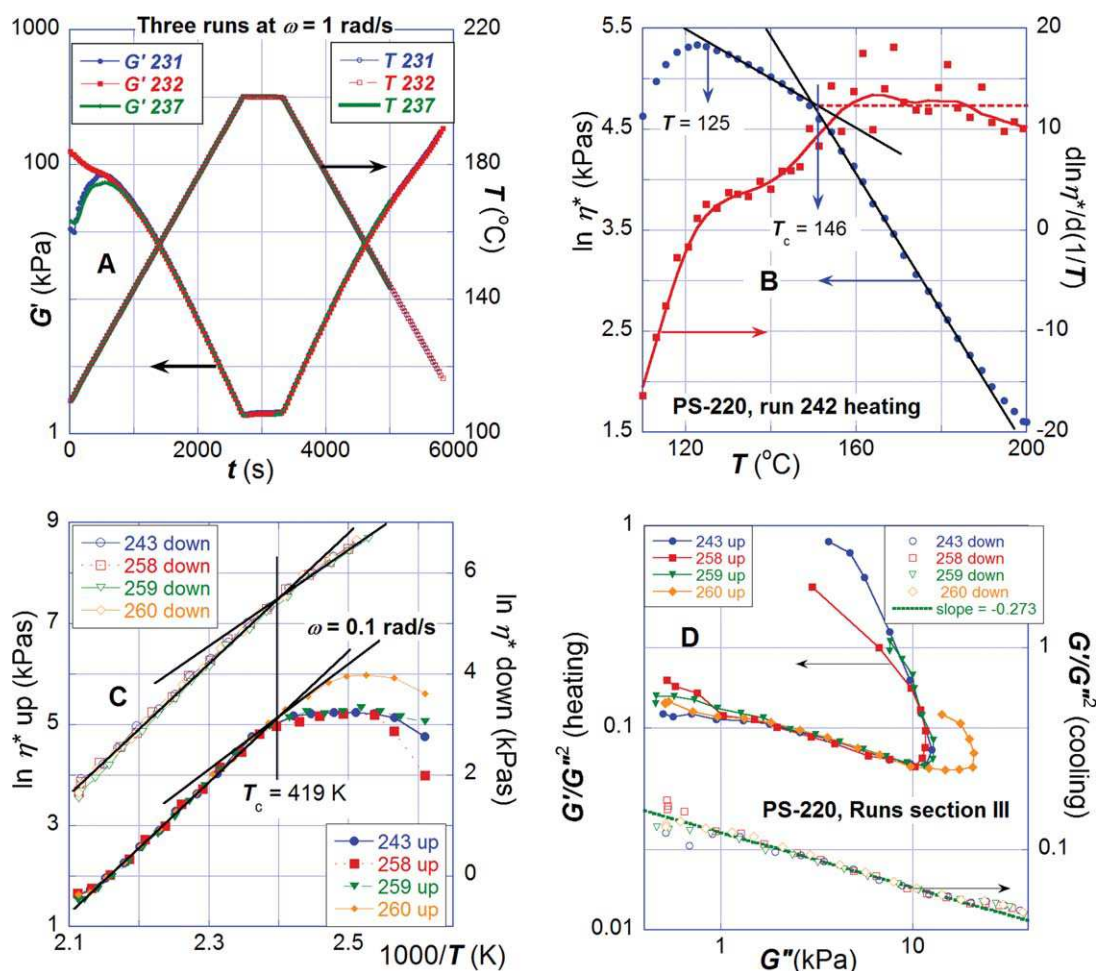
FIGURE 6 Examples of the dynamic melt flow results: (A) time-dependent variation of T and the storage modulus for three runs in Series I. (B) Complex viscosity and its derivative in Series II; $T_c \approx 146$ is indicated. (C) Complex viscosity versus reciprocal temperature for the four runs of Series III. Lower curves represent data collected upon heating, the upper ones on cooling; the crossover-T is common, T_c, = 146 ± 2 °C. (D) Doi-Edwards plot for Series III data. The upper curves were obtained on heating from 110 to 200 °C, the lower set on cooling from 200 °C; for $1 < G''(\text{kPa}) < 11$ the behavior is common with decreasing slope of −0.273.

V versus T dependence for melts may not represent T_g; notably, the volume expansion at $T < T_g$ is so large that a structural rearrangement in the vitreous state is less probable than within supercooled liquid near vitrification. It is noteworthy that in Figure 3(D), while at low $P = 0.1$ or 10 MPa, $T_g = 361.3 \pm 1$ K for all three polymers, at high pressure (calculated for $P = 190$ MPa), the values for PS-686, PS-667, and PS-1301 are: $T_g = 432, 418,$ and 422, respectively, making the T_g value of PS-686 unduly high.[35] Furthermore, the volume expansion within the T_g region implies that the isobaric quenching leads to a nonequilibrium reduction of V.

By contrast with isobaric cooling in Figure 3(A), the high-P isobaric heating in Figure 3(B) results in a smooth, linear increase of PS-667 volume on both sides of T_g. It is noteworthy that only these measurements results in a constant slope of $\ln V$, that is, in $\alpha \approx$ constant below and above T_g at low and at high P. Figure 3(C) displays $\ln V$ and α for PS-1301 measured by the isothermal heating method. The low-P data in Figures 3(B) and 3(C) are superposable, but the high-P

ones are not. By contrast with $\alpha \approx$ constant in Figure 3(B), the dependence in Figure 3(C) shows that $\alpha = 0$ within the transition zone **T**. As it was pointed out,[39,46] the **T**-zone starts at $T = T_g(P = 0.1 \text{ MPa}) \approx 361$ K and ends at $T = T_g(P = 190 \text{ MPa}) \approx 422$ K. This behavior may originate in the revitrification of molten polymer under pressure when isothermally increasing P within the cited above range of temperature.[47]

The compressibility coefficients, κ, in Figure 3(D) are in relatively good agreements with V and α dependencies for the three polymers. The rapid isobaric cooling of PS-686 resulted in slightly lower melt compressibility, thus larger V then those of PS-667 or PS-1301. The "abnormal" high-P behaviors of PS-686 and to some extent of PS-1301 within the transition **T**-zone are also evident. However, for the present discussion on the melt structure above T_g, the low-pressure compressibility are highly significant. The original publications[34,46,48] show in detail that as T increases above T_g, κ has two slopes on both sides of $T_c \approx T_{LL}$. Comparing the

three κ versus T dependencies in Figure 3(D), one may note that the crossover transition is evident from the three test procedures, but within the temperature range: $T_g < T < T_c$, the compressibility is not identical. For example, rapid cooling of PS-686 results in lower slope and behavior shifted to lower temperatures. By contrast, the slow isobaric heating of PS-667 reverses those tendencies. These changes can be understood considering the variable PS structures within this T-zone.

In short, the three PVT measurement procedures were: (1) isobaric cooling at a rate $q = 10$ °C/min, (2) isobaric, and (3) isothermal heating at a rate $q = 0.035$–0.050 °C/min. The melt data in Figure 3(A) may not be at the thermodynamic equilibrium. Method (2) results in the simplest dependencies, with constant values of α and regular variation of κ for glass and melt above T_c. The resulting V and α data [Fig. 3(B)] superpose on those obtained by method (3) [Fig. 3(C)] except for the **T**-region. Thus, the slow isobaric heating is preferred over the standard procedure as it leads to reproducible PVT results on both sides of T_g without the complexity of the **T**-region. The similarity of the dependencies displayed in Figures 3(B) and 3(C) is noteworthy. The thermal expansion coefficients, $\alpha = \alpha(T)$, measured isobarically or isothermally on heating, are nearly superimposable. The coefficient increases with T across T_g up to $T_c \approx 1.14 T_g$ where it becomes constant, indicating an equilibrium melt. Thus, the three methods lead to different V, α, and κ behaviors not only at $T < T_g$. However, the differences are undetectable at $T > T_c$. It is significant that the secondary transitions (e.g., glass–glass transition T_β or liquid–liquid transition T_{LL} or T_c) are as weak as being invisible on $V = V(T)$ plots.

The dynamic shearing of glass and melt were conducted at ambient pressure. The specimens were compression molded at about 200 °C and then cooled down as described in the Experimental section. The viscoelastic measurements of molded PS-1301 specimens were performed at constant frequency, $\omega = 1$ rad/s while heating from about 304 to 405 K at the rates: $q = 1, 2, 3$ and 4 °C/min; thus, as $T_g = 378 \pm 0.2$ K, the tests were conducted at: $-74 \leq [T - T_g](^oC) \leq 27$.

The T-dependences of the dynamic storage and loss moduli (respectively E' and E'') tested at $q = 1$ and 3 are presented in Figure 4. Near T_g, on both its sides, the derivatives dE'/dT and dE''/dT show clear difference of behavior, especially for the quenched (qu) and annealed (an) specimens. Figures 5(A) and 5(B) displays the tensile moduli ratios of the qu-to-an specimens, thus $E'(qu)/E'(an)$ and $E''(qu)/E''(an)$, respectively. It is noteworthy that the former ratio is about 50% larger than that of the latter, but they both reach maxima at $T/T_g \approx 1.02$, or about 8 °C above T_g. The largest difference of behavior of "qu" from "an" specimen was observed for the fastest heating, $q = 4$ °C/min, the smallest for the slowest one, $q = 1$ °C/min, indicating that during the temperature increase above T_g the solid aggregate structures dissipate with time. However, even 20 °C above T_g the reproducible data indicate different behavior of differently prepared specimens, apparently having different structures of the percolating clusters. In other words, as $T_c - T_g = 41$ °C, the viscoelastic behavior of molten PS may be affected by specimen history up to half-way from T_g to T_c.

The Melt Region and T_c

The PVT and flow behavior of molten polymer are related through the free volume fraction, f, or the hole content, h. Thus, one may expect that the P and T dependence of the melt viscosity ($\eta_{\sigma_{ij}=\text{const}}$ is the zero-shear or constant stress quantity) will follow the dependence: [49–52]

$$\ln \eta_{\sigma_{ij}=\text{const}} = a_0 + a_1 Y_s; \quad Y_s \equiv 1/(h+a_2) \quad (5)$$

Equation 5 implies that $\eta_{\sigma_{ij}=\text{const}}$ is a function of T and P only through $h = h(T, P)$, for example, computed from the Simha–Somcynsky equation of state (S–S eos).[53] For low molecular weight liquids and their mixtures (e.g., n-paraffins or silicon oils), good superposition was found in wide ranges of T (e.g., 20 to 204 °C) and P (e.g., 0.1 to 500 MPa). The parameter a_0 in eq 5 is a scaling one, while $a_1 = 0.79 \pm 0.01$ and $a_2 = 0.07$ were found common for all the analyzed liquids; the latter is only needed for the linearization of dependence and hence fundamentally unimportant.

Few years ago eq 5 was applied to eight molten polymers whose PVT and capillary shear viscosity $\eta = \eta(P, T)$ were determined up to $P = 70$ MPa.[54] By contrast with the previously found superposition for solvents and silicone oils, the polymer data plotted as log η versus $1/h$ did not follow a "master curve." The discrepancy could be eliminated by introducing an empirical reducing pressure, $P_R^* = \zeta P^*$, with a fudge factor, $\zeta \approx 1$ to 2.1, indicating variable strength of the Lennard–Jones maximum attractive energy, ε^*, caused by variability of structures/aggregations at $T_g \leq T \leq T_c$. The TFT model supports this explanation, as the liquid entrapped within the aggregates would not contribute to flow.

The presence of structure at $T_g \leq T \leq T_{LL}$ was also postulated by Boyer and his coworkers. For example, it was noted that the polymer melt should be processed only above T_{LL} as only then it behaves as a regular liquid.[55–58] This postulate agrees well with the observed constancy of the thermal expansion coefficient, $\alpha = $ const at $T > T_{LL}$ as well as the reported changes of flow behavior at this T_{LL}. For the practical reasons, T_{LL} is the lowest processing temperature for acceptable surface and performance of extruded or injection-molded articles.[58]

The T_{LL} concept passed through a series of transformations and redefinitions, but it is undeniable that its numerical values are close to those of T_c. However, while T_{LL} was considered a proportional or a linear function of T_g, the T_c was found dependent on M_n and the fragility index, m; for PS the reported value is: $T_c/T_g = 1.15 \pm 0.09$ (the error was calculated for organic glass formers). TFT postulates an exponential formation of twinkling solid aggregates at $T < T_c$. Accordingly, the AFM images taken at $T/T_g = 1.05$ showed relatively low concentration of aggregates[32] while the infinite percolation cluster is expected at $T = T_g$.

Empirically, the transition temperature, T_g or T_{LL}, linearly varies with reciprocal number-average molecular weight:[59]

$$T_{g,LL} = T_{g,LL}^{\infty} - K_{g,LL}/\bar{M}_n \qquad (6)$$

The eq 6 parameters depend on polydispersity, for example, for narrow molecular distribution PS: $T_{LL}^{\infty} = 417.9$ (K), $K_{LL} = 105$ (K kDa), while $T_g^{\infty} = 386.1$(K), $K_g = 97.4$ (K kDa). Thus, the ratio $T_{LL}/T_g = 1.083 \pm 0.003$ is nearly independent of $\bar{M}_n$, and $T_{LL} \approx T_g + 32$. For the commercially polydispersed PS, these quantities are: $T_c/T_g \approx 1.14 \pm 0.02$ and $T_c - T_g \approx 44 - 58\,^{\circ}$C.

In this investigation, the dynamic melt flow of the low molecular weight PS-220 was studied by heating the specimens from $T \approx T_g + 22 = 383$ to 473 K, annealing at that temperature and then cooling to about 390 ± 1 K [see Fig. 6(A) and Table 2]. During this heating–annealing–cooling cycle, the storage shear modulus, log G', of Series I samples initially increased, went through a local maximum, decreased, was constant at 200 $^{\circ}$C, and then nonlinearly increased on cooling. Good reproducibility of data was obtained. For the purpose of this publication, the initial part is most important, during which the dependence goes through a peak or [e.g., run #232 in Figure 6(A)] a shoulder. Depending on the heating rate ($q = 1 - 3\,^{\circ}$C/min), this stage was reached at $T \approx 397 \pm 3$ K, that is, at $T/T_g = 1.10 \pm 0.01$, thus as it will be shown later, half way between T_g and T_c. The good quality of specimens recovered after the test indicates that this effect is not an artifact but the true material performance most likely caused by relaxation of the residual stresses engendered during the specimen loading so close to T_g. Tests summary in Table 2 indicates that none of the examined parameters, that is, specimen thickness, frequency, magnitude of the normal force used during sample loading, or T-span, correlate with the rheological response during the initial heating. The source of this behavior must be formation of a fragile structure during the specimen preparation, which is being destroyed at about $T - T_g = 19 \pm 3\,^{\circ}$C, and it is not rebuilt on cooling.

For detecting a transition in rheological data (e.g., T_c), Stickel et al. suggested using differentiated VFTH expression in the form:[60,61]

$$[d(\ln\eta^*)/d(1/T)]^{-1/2} = B^{-1/2}(1 - T_o/T) \qquad (7)$$

where B and T_o are constants of the VFTH equation. However, eq 7 requires positive derivative: $d(\ln\eta^*)/d(1/T \geq 0)$, which [as shown in Fig. 6(A)] is not always observable. Therefore, in Figure 6(B), the complex viscosity and its temperature gradient are plotted as $\ln\eta^*$ and $d(\ln\eta^*)/d(1/T)$ versus T. The change of slope of these functions indicates the transition temperature, $T_c = 419 \pm 1 = T_g + 41$ K, thus higher than the peak or shoulder of the η^* versus T function in Figure 6(B). Similar analysis was carried out for the heating and cooling temperature sweeps of other runs. Figure 6(C) displays $\ln\eta^*$ versus $1/T$ for Series III measurements. The average transition temperature for the heating and cooling samples, $T_c = 419 \pm 3$ K, is indicated and the numerical values are listed in Table 2. In this Series III measurements, on heating, the dependence
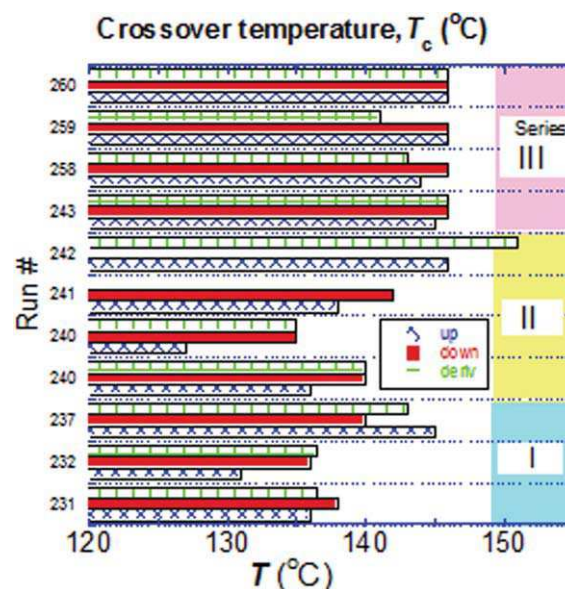

FIGURE 7 Crossover temperature for all the test runs as determined from the flow curves on heating, on cooling and from the first derivatives of complex viscosity, d ln η^*/$d(1/T)$.

$\ln\eta^*$ versus T is common with a change of slope at T_c, not as well defined during the cooling sweeps. As listed in Table 2, the only difference between this series of samples and the one shown in Figure 6(B) is the heating rate, thus the latter sample could join the common behavior sooner than the heated twice as fast samples of Series III.

Figure 6(D) illustrates the common behavior of Series III samples plotted as suggested by the Doi and Edwards's equation for the terminal zone:[62]

$$G'/G''^2 = (6M_e/5\rho RT)\left[1 + (G'/G'')^2\right] \qquad (8)$$

where M_e is the entanglement molecular weight, ρ is density, and R is the gas constant. At constant T, the dependence predicts that $G'/G''^2 = $ const., whereas the experimental plot shows that, on heating or cooling, the function decreases with T at a slope of -0.273. Evidently, both V and $G''/G' \equiv \tan\delta$ depend on T [viz. d $\ln V/dT \cong 0.265$, and d $\ln(\tan\delta)/dT \cong 0.0414$]. Both branches, on heating or on cooling a common behavior shows within the range of $G'' = 1$–11 kPa, with the higher value $T \approx 145 \pm 1\,^{\circ}$C, in agreement with $T_c = 146 \pm 3\,^{\circ}$C determined above.

Figure 7 displays the spread of T_c values. The analysis of the T-sweeps in heating and cooling cycles was used for determining T_c for Series I–III with scatter $\leq 4\,^{\circ}$C, giving the ratio $T_c/T_g = 1.14$, 1.14, and 1.16 (± 0.01), respectively. These values compare well with the earlier reports summarized in Table 3, which lists T_{LL}, T_c, T_g, and their ratios for commercial polydispersed and often lubricated PS. It is significant that, while, for the nearly monodispersed, anionic PS, the ratio: $T_g/T_c \approx 1.08$, for the commercial polydispersed and

TABLE 3 Crossover and Glass Transition Temperature for Commercial PS

M_n (kDa)	T_{LL} or T_c (K)	T_g (K)	T_c/T_g	Comments	Refs.
20.4	414	385	1.08	DMTA	63
10.3	401	378	1.06		
2.03	387	339	1.14		
51	435.8	372	1.17	*PVT*	64
4	401.1	331.5	1.21	Viscosity and polarization	3
37	417.1	365.9	1.14		
390	438.1	373.1	1.17		
3.5	388.1	330.1	1.18	Melt viscosity	65
9.2	410.1	357.1	1.15		
16.2	413.1	366.1	1.13		
29.5	424.1	372.1	1.14		
47.5	423.1	373.1	1.13		
51.4	424.1	373.1	1.14		
125	429.1	373.1	1.15		
267	431.1	373.1	1.16		
10	420	365	1.15	Light scattering	8, 66
56	419 ± 3	360.8	1.16 ± 0.01	Dynamic flow	This work

lubricated PS, the ratio is $T_c/T_g \approx 1.14 \pm 0.01$. Boyer reported that experimentally:[2]

$$T_{LL} = 30.47 + 1.087 T_g \qquad (9)$$

For high molecular weight PS with $T_g = 105$ °C, eq 9 gives the ratio: $T_{LL}/T_g = 1.17$.

SUMMARY AND CONCLUSIONS

The aim of this article is the analysis of physical behavior of molten PS, especially in the vicinity of T_g. In particular, the studies focus on the effect of the specimen preparation and measurements of the *PVT* and rheological behavior. Based on the collected data, the following observations may be made:

1. At low temperatures, $T < T_\beta$, the dynamic tensile moduli do not depend on the method of specimen preparation and measurements. Only above this secondary glass/glass transition, the moduli of annealed, quenched, and slow-cooled specimens show different temperature dependencies.
2. The *PVT* behavior at $T < T_g$ show large differences, depended on the test procedure. The largest transient zone, **T**, was observed for rapid isobaric cooling, smaller for the standard isothermal heating and none for the slow isobaric heating. Thus, these measurements evidenced the influence of the cooling/heating rates on specific volume and its derivatives.
3. The slow-heating isobaric and isothermal tests yielded superposable *V*-behavior at $T > T_g$. At higher temperatures, the derivatives, α and κ, indicated different behavior of the molten polymer on the two sides of the crossover temperature, T_c.
4. The viscoelastic *T*-scan at $\omega = 1$ rad/s across the T_g-region confirmed the expectation. Of the three types of compression-molded specimens, the quenched ones showed the highest moduli while the annealed the lowest. The maxi-

mum of the tensile moduli ratios: $E'(qu)/E'(an)$ and $E''(qu)/E''(an)$ was at $T = T_g + 8$ °C. The difference of rigidity was detectable at $T \geq T_g + 20$ °C, that is, half way to T_c. Thus, the data make it evident that, at $T > T_g$, the polymer is not always at the thermodynamic equilibrium.
5. The melt rheology *T*-scans started at $T \approx T_g + 22$ °C, thus above the region where the viscoelastic tests detected large effects of the specimen preparation and testing. The initial heating showed effects related to the method of specimen preparation and the normal stress imposed during loading. The tests yielded consistent values of $T_c = 419 \pm 2$ K, or $T_c/T_g = 1.16 \pm 0.01$, in agreement with earlier reports.
6. The presented macro-scale thermodynamic and rheological data show that in agreement with the earlier theoretical and experimental evidences the molten state above T_g is dynamic and heterogeneous in nature, with the structure dependent on the initial state and elapsed time.[2–5,22,23,31,32,55,67,68]

REFERENCES AND NOTES

1 Simha, R.; Roe, J. M.; Nanda, V. S. *J. Appl. Phys.* **1972**, *43*, 4312–4317.

2 Boyer, R. F. In Encyclopedia of Polymer Science and Technology: Plastics, Resins, Rubbers; Mark, H. F., Ed.; Wiley-Interscience: New York, **1977**; Suppl. Vol. *2*, pp 745–839.

3 Boyer, R. F. In Polymer Yearbook 2; Pethrick, R. A., Ed.; Harwood Academic Publishers: Chur, **1985**; pp 233–343.

4 Boyer, R. F. *J. Macromol. Sci. Phys.* **1980**, *B18*, 461–553.

5 Boyer, R. F. InOrder in the Amorphous "State" of Polymers; Keinath, S. K.; Miller, R. L.; Rieke, J. K., Eds.; Plenum: New York, **1987**; pp 135–185.

6 Spencer, R. S.; Dillon, R. E. *J. Colloid Sci.* **1949,** *4*, 241–255.

7 Boyer, R. F.; Heeschen, J. P.; Gillham, J. K. *J. Polym. Sci. Polym. Phys. Ed.* **1981,** *19*, 13–21.

8 Kisliuk, A.; Mathers, R. T.; Sokolov, A. P. *J. Polym. Sci. Part B: Polym. Phys.* **2000,** *38*, 2785–2790.

9 Surovtsev, N. V. *J. Phys. Condens. Matter* **2007,** *19*, 196101 (8 pp).

10 Götze, W.; Sjogren, L. *Rep. Prog. Phys.* **1992,** *55*, 241–370.

11 Jäckle, J. *Rep. Prog. Phys.* **1986,** *49*, 171–231.

12 Kanaya, T.; Kawaguchi, T.; Kaji, K. *Macromolecules* **1999,** *32*, 1672–1678.

13 Kanaya, T.; Kaji, K. *Adv. Polym. Sci.* **2001,** *154*, 87–141.

14 Binder, K.; Baschnagel, J.; Paul, W. *Prog. Polym. Sci.* **2003,** *28*, 115–172.

15 Casalini, R.; Roland, C. M. *Phys. Rev. B* **2005,** *71*,014210–1–014210–10.

16 Roland, C. M.; McGrath, K. J.; Casalini, R. *J. Non-Cryst. Solids* **2006,** *352*, 4910–4914.

17 Kunal, K.; Robertson, C. G.; Pawlus, S.; Hahn, S. F.; Sokolov, A. P. *Macromolecules* **2008,** *41*, 7232–7238.

18 Kunal, K.Influence of Chemical Structure and Molecular Weight on Fragility in Polymers, Ph.D. Thesis, The University of Akron, Akron, OH, August, **2009.**

19 Robertson, C. G.; Roland, C. M. *J. Polym. Sci. Part B: Polym. Phys.* **2004,** *42*, 2604–2611.

20 Ngai, K. L. *J. Non-Cryst. Solids* **2000,** *275*, 7–51.

21 Ngai, K. L. *J. Phys. Condens. Matter* **2003,** *15*, S1107–S1125.

22 Wool, R. P. *J. Polym. Sci. Part B: Polym. Phys.* **2008** *46*, 2765–2778; DOI: 10.1002/polb.21596.

23 Robertson, R. E. *Annu. Rev. Mater. Sci.* **1975,** *5*, 73–97.

24 Neher, R. A.; Mecke, K.; Wagner, H. *J. Stat. Mech.* **2008,** P01011 (14 pgs.); DOI: 10.1088/1742–5468/2008/01/P01011.

25 Lyngaae-Jørgensen, J.; Utracki, L. A. *Macromol. Chem. Macromol. Symp.* **1991,** 48/49, 189–209.

26 Simha, R.; Weil, C. E. *J. Macromol. Sci. Phys.* **1970,** *B4*, 215–226.

27 McKinney, J. E.; Simha, R. *Macromolecules* **1974,** *7*, 894–901.

28 McKinney, J. E.; Simha, R. *Macromolecules* **1976,** *9*, 430–441.

29 Simha, R. *Rheol. Acta* **1975,** *14*, 12–18.

30 Simha, R. *Macromolecules* **1977,** *10*, 1025–1030.

31 Wool, R. P.; Campanella, A. *J. Polym. Sci. Part B: Polym. Phys.* **2009,** *47*, 2578–2590; DOI: 10.1002/polb.21882.

32 Stanzione, J. F., III; Strawhecker, K. E.; Wool, R. P. *J. Non-Crystal. Solids* **2011,** *357*, 311–319; DOI: 10.1016/j.jnoncrysol. 2010.06.041.

33 Zoller, P.; Walsh, D. Standard Pressure-Volume-Temperature Data for Polymers; Technomic: Lancaster-Basel, **1995.**

34 Utracki, L. A. *J. Polym. Sci. Part B: Polym. Phys.* **2007,** *45*, 270–285; DOI: 10.1002/polb.

35 Quach, A.; Simha, R. *J. Appl. Phys.* **1971,** *42*, 4592–4606.

36 Qiu, H.; Bousmina, M.; Dealy, J. M. *Rheol. Acta* **2002,** *41*, 87–92; DOI: 10.1007/s003970200008.

37 Utracki, L. A. *Polymer* **2005,** *46*, 11548–11556; DOI:10.1016/ j.polymer.2005.10.020.

38 Tanoue, S.; Utracki, L. A.; Garcia-Rejon, A.; Tatibouët, J.; Cole, K. C.; Kamal, M. R. *Polym. Eng. Sci.* **2004,** *44*, 1046–1060; DOI: 10.1002/pen.20098.

39 Utracki, L. A. *J. Polym. Sci. Part B: Polym. Phys.* **2008,** *46*, 2504–2518; DOI: 10.1002/polb.21413.

40 SEC of PS-220 was determined by Dr. L. E. Daigneault **1994.**

41 Schmidt, M. Macroscopic volume and free volume of polymer blends and pressure-densified polymers. Ph.D. Thesis, Chalmers University, Göteborg, Sweden **2000.**

42 Struik, L. C. E. Physical Aging in Amorphous Polymers and Other Materials; Elsevier: Amsterdam, **1978.**

43 Quach, A.; Simha, R. *J. Phys. Chem.* **1972,** *76*, 416–421.

44 Hellwege, K.-H.; Knappe, W.; Lehmann, P. *Kolloid-Z. Z. Polymere* **1962,** *183*, 110–120.

45 Breuer, H.; Rehage, G. *Kolloid-Z. Z. Polymere* **1967,** *216–217*, 159–179.

46 Utracki, L. A. *Eur. Polym. J.* **2009,** *45*, 1891–1903; DOI: 10.1016/j.eurpolymj.2009.04.009.

47 Pionteck, J.The Explanation Proposed at the PPS Regional Meeting, Istanbul, 20–23 October, **2010.**

48 Utracki, L. A. *Polym. Degrad. Stab.* **2010,** *95*, 411–421; DOI: 10.1016/j.polymdegradstab.2009.07.020.

49 Utracki, L. A. *Polym. Eng. Sci.* **1983,** *23*, 446–452.

50 Utracki, L. A. *Can. J. Chem. Eng.* **1983,** *61*, 753–758.

51 Utracki, L. A. *J. Rheol.* **1986**, 30, 829–841; the *JR* issue contains papers presented at the Symposium on Applications of Equations of State in Rheology, organized by Dr. B. Hartmann and edited by him.

52 Utracki, L. A. *Polym. Eng. Sci.* **1985,** *25*, 655–668.

53 Simha, R; Somcynsky, T. *Macromolecules* **1969,** *2*, 342–350.

54 Utracki, L. A.; Sedlacek, T. *Rheol. Acta* **2007,** *46*, 479–494; DOI: 10.1007/s00397–006-0133-z.

55 Hyun, K. S.; Boyer, R. F. In Encyclopedia of Polymer Science and Technology: Plastics, Resins, Rubbers; Mark, H. F., Ed.; Wiley-Interscience: New York, **1970; Vol.** 13, 349–375.

56 Stadnicki, S. J.; Gillham, J. K. *J. Appl. Polym. Sci.* **1976,** *20*, 1245–1275.

57 Keinath, S. E.; Boyer, R. F. *J. Appl. Polym. Sci.* **1981,** *26*, 2077–2085.

58 Boyer, R. F. *Polym. Eng. Sci.* **1979,** *19*, 732–748.

59 Glandt, C. A.; Toh, H. K.; Gillham, J. K.; Boyer, R. F. *J. Appl. Polym. Sci.* **1976,** *20*, 1277–1288.

60 Stickel, F. E.; Fischer, W.; Richert, R. *J. Chem. Phys.* **1995,** *102*, 6251–6257.

61 Stickel, F. E.; Fischer, W.; Richert, R. *J. Chem. Phys.* **1996,** *104*, 2043–2055.

62 Doi, M.; Edwards, S. F. *J. Chem. Soc. Faraday Trans. 2* **1978,** *74*, 1802–1817.

63 Cowie, J. M. G.; McEwen, I. J. *Polymer* **1979,** *20*, 719–724.

64 Boyer, R. F. *Macromolecules* **1982,** *15*, 1498–1504.

65 Boyer, R. F. *Eur. Polym. J.* **1981,** *17*, 661–673.

66 Novikov, V. N.; Sokolov, A. P.; Strube, B.; Surovtsev, N.; Duval, E.; Mermet, A. *J. Chem. Phys.* **1997,** *107*, 1057–1065.

67 Long, D.; Lequeux, F. *Eur. Phys. J.* **2001,** *E4*, 371–387.

68 Merabia, S.; Long, D. *Eur. Phys. J.* **2002,** *E9*, 195–206; DOI 10.1140/epje/i2002-10084-2.